doi: 10.1111/j.1365-3121.2009.00877.x

Sm–Nd isotopic mapping of lithospheric growth and stabilization in the eastern Kaapvaal craton

Blair Schoene,[1] Francis O. L. Dudas,[1] Samuel A. Bowring[1] and Maarten de Wit[2]

[1]*Department of Earth, Atmospheric and Planetary Sciences, Massachusetts Institute of Technology, Cambridge, MA 02139, USA;* [2]*African Earth Observatory Network and Department of Geological Sciences, University of Cape Town, Rondebosch 7701, South Africa*

ABSTRACT

Whole-rock Sm–Nd isotope systematics of 79 Archean granitoids from the eastern Kaapvaal craton, southern Africa, are used to delineate lithospheric boundaries and to constrain the timescale of crustal growth, assembly and geochemical differentiation *c.* 3.66–2.70 Ga. Offsets in ε_{Nd} values for 3.2–3.3 Ga granitoids across the Barberton greenstone belt (BGB) are consistent with existing models for *c.* 3.23 Ga accretion of newly formed lithosphere north of the BGB onto pre-existing *c.* 3.66 Ga lithosphere south of the BGB along a doubly verging subduction margin. The Nd isotopic signature of *c.* 3.3–3.2 Ga magmatic rocks show that significant crustal growth occurred during subduction–accretion. After *c.* 3.2 Ga, however, the Nd signature of intrusive rocks *c.* 3.1 and 2.7 Ga is dominated by intracrustal recycling rather than by new additions from the mantle, signalling cratonic stability.

Terra Nova, 21, 219–228, 2009

Introduction

Models of the structure and composition of continental lithosphere are constrained by the integration of geological and geophysical data and rely on the relatively rare occurrence of xenolith bearing volcanic rocks. Alternatively, the geochemistry and isotopic characteristics of exposed igneous rocks can be viewed as probes of their source regions and therefore provide insight into magmatic processes and lithospheric structure. In particular, Sm–Nd isotope systematics can be used to constrain the time-scales of early crust-mantle segregation and subsequent magmatic and geochemical differentiation of the lithosphere (DePaolo and Wasserburg, 1976a; DePaolo, 1980; Nutman *et al*., 1993). In addition, differences in the Nd signature of plutonic rocks can be used to identify important lithospheric boundaries that may not be recorded in the ages of rocks at the surface (Bennett and DePaolo, 1987; Milisenda *et al*., 1988; Davis and Hegner, 1992; Dickin, 2000).

The Kaapvaal craton in southern Africa is one of the most extensively studied fragments of Archean lithosphere and has long served as a crucible for the development of models for Archean crustal growth (Viljoen and Viljoen, 1969; Green, 1975; Anhaeusser, 1983; Richardson *et al*., 1984; de Wit *et al*., 1992; Grove and Parman, 2004; Moyen *et al*., 2006). However, high-resolution seismic studies and the occurrence of xenolith bearing kimberlites are restricted to the mostly Neoarchean central and western craton, whereas the best exposed and oldest basement rocks occur in the eastern craton (Carlson *et al*., 2000; Schmitz *et al*., 2004). To bridge this gap in knowledge of the 3-D petrologic and geochemical structure of the eastern Kaapvaal craton, we analysed whole-rock Sm–Nd isotopic systematics of 79 *c.* 3.66–2.70 Ga plutonic and orthogneiss samples from a ~200-km long transect across potential Mesoarchean lithospheric discontinuities. We use these data to identify and refine lithospheric boundaries and to evaluate crustal growth and differentiation as a function of time. These new data, which nearly quadruple the existing database for such rocks in the region, lead to improved tectonic models for the assembly and stabilization of the eastern Kaapvaal craton.

Correspondence: Blair Schoene, Department of Mineralogy, University of Geneva, Rue des Maraîchers 13, Geneva CH-1205, Swtizerland. Tel.: +41 22 379 31 76; fax: +41 22 379 32 10; e-mail: blair.schoene@unige.ch

Geological setting and sampling

The present-day crustal architecture of the Kaapvaal craton flanking the Barberton greenstone belt (BGB) is commonly explained within the context of a *c.* 3.2–3.3 Ga NW–SE directed subduction–accretion event, which is recorded by coeval syntectonic magmatism, syn-contractional to strike–slip basin development, and high-grade metamorphism (Kröner *et al*., 1991; de Wit *et al*., 1992; Kamo and Davis, 1994; Lowe, 1994; de Ronde and de Wit, 1994; Lowe and Byerly, 1999; de Ronde and Kamo, 2000; Stevens *et al*., 2002; Diener *et al*., 2005; Dziggel *et al*., 2005; Moyen *et al*., 2006). This period was followed by *c.* 100 Ma of continued transform boundary deformation, culminating in *c.* 3.1 Ga granitic magmatism and differential exhumation of rocks on reactivated faults (Westraat *et al*., 2005; Schoene and Bowring, 2007; Schoene *et al*., 2008).

It has been inferred that *c.* 3.23 Ga deformation was the result of the amalgamation of at least two microcontinental blocks, with the Saddleback-Inyoka fault system (SIFS) within the BGB representing a lithospheric suture zone (Fig. 1; de Wit *et al*., 1992; de Ronde and de Wit, 1994; Heubeck and Lowe, 1994; Lowe and Byerly, 1999). However, there is considerable uncertainty about the boundaries of the different terranes, their nature with depth, and how they were amalgamated. The 3.66–3.45 Ga mafic-silicic banded gneiss of the Ancient Gneiss Complex (AGC; Jackson, 1984; Compston and Kröner, 1988; Kröner *et al*., 1989; Kröner and Tegtmeyer, 1994) to the south of the BGB is one of the terranes (Jackson *et al*., 1987) and it was intruded

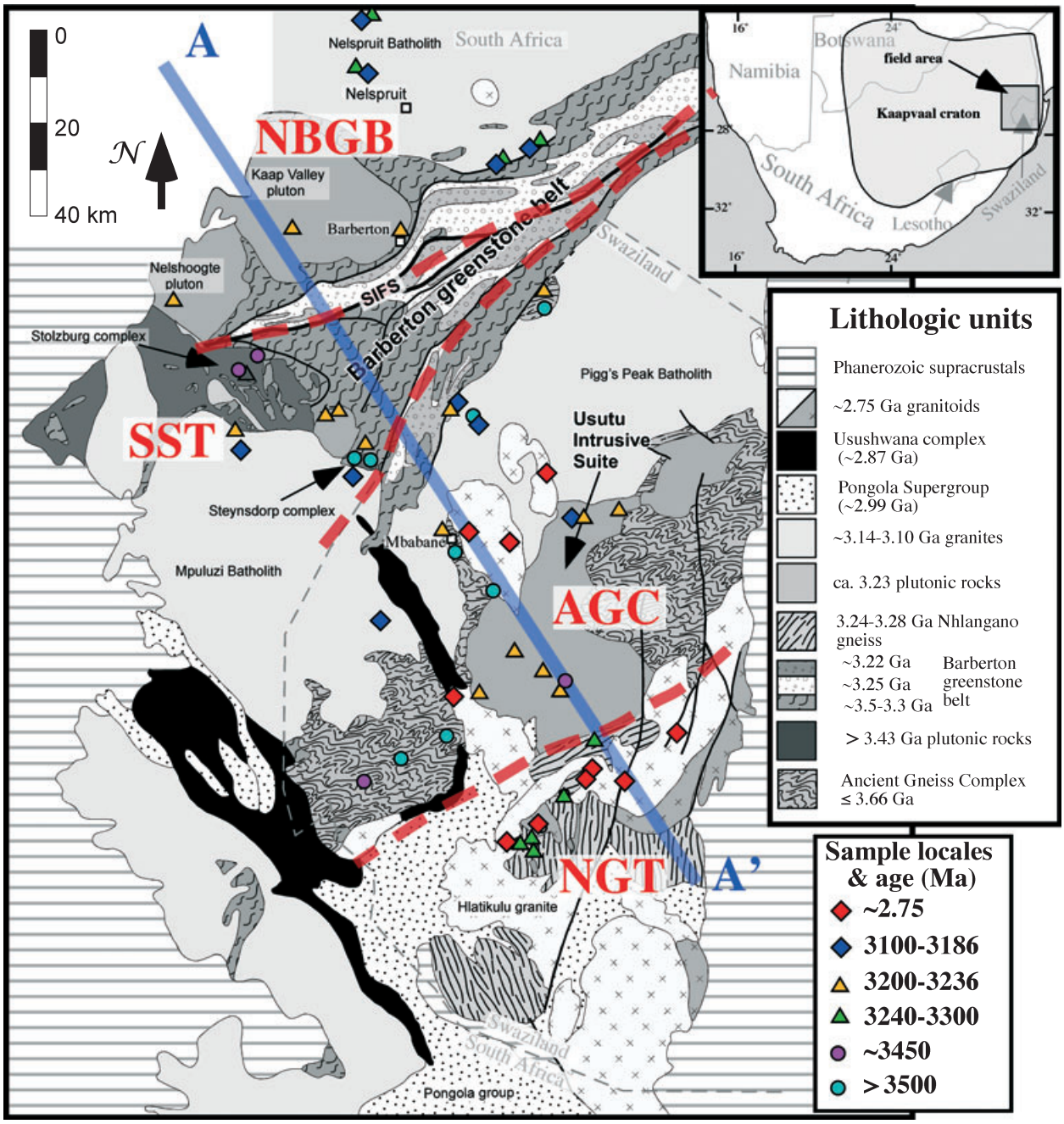

Fig. 1 Geological map of the eastern Kaapvaal craton, showing sample locations and crystallization ages from this study. Also shown are the extents of lithospheric blocks: NBGB, rocks north of the Barberton Greenstone Belt; SST, the Stolzburg and Steynsdorp Terrane; AGC, Ancient Gneiss Complex; NGT, Nhlangano Gneiss Terrane. Terrane boundaries are denoted by red dashed lines. SIFS, Saddleback-Inyoka Fault System. A–A′ denotes the line onto which the samples were perpendicularly projected in Fig. 2. Map compiled from Wilson, 1982; de Wit, 1982; de Ronde *et al.*, 1994; Lowe and Byerly, 1999; Schoene *et al.*, 2008; Schoene and Bowring (in revision).

by granodiorites to tonalites forming the Usutu Intrusive Suite from 3236 to 3220 Ma that record NW–SE compression in magmatic fabrics (Schoene and Bowring, in revision). Further south, a suite of complexly deformed orthogneisses called the Nhlangano gneiss (NGT), are *c.* 3240–3280 Ma (Schoene and Bowring, in revision), although its relationship to the AGC is not well-understood. The terrane to the north of the BGB has been suggested to represent a young island-arc type continental fragment that was accreted onto the AGC *c.* 3.23 Ga along a NE-trending boundary (de Wit *et al.*, 1992), consistent with zircon dates from the

Table 1 Sample summary and Sm–Nd data.

Sample description								Analytical data						
Name (a)	Rock unit (b)	Lithology (c)	Latitude (d)	Longitude (d)	Terr. (d)	Age (e)	Ref. (e)	[Sm] (f)	[Nd] (f)	$\frac{^{147}Sm}{^{144}Nd}$ (g)	$\frac{^{143}Nd}{^{144}Nd}$ (g)	± (h)	$\varepsilon_{Nd}(0)$ (i)	$\varepsilon_{Nd}(t)$ (i)
c. 2.73 Ga granites														
WKC0066	Mbabane pluton	Co. grained granite	26.3046	31.1551	AGC	2690	*1	9.66	59.52	0.09815	0.510563	6	−40.47	−6.38
WKC0071	Hlatikulu granite	Med. grained granite	26.7484	31.3851	NGT	2730	2	7.25	41.76	0.10493	0.510639	6	−39.00	−6.56
WKC0078	Hlatikulu granite	Med. grained granite	26.7556	31.4540	NGT	2730	2	9.56	59.28	0.09753	0.510499	6	−41.73	−6.67
WKC0081	Ngwempisi granite	Co. grained granite	26.6000	31.1614	AGC	2730	**3	16.44	105.68	0.09404	0.510499	8	−41.72	−5.48
EKC02-25	Malendela pluton	Co. grained granite	26.2029	31.3340	AGC	2730	**3	13.63	94.27	0.08739	0.510235	8	−46.87	−8.23
EKC02-30	Mbabane pluton	Co. grained granite	26.3302	31.2626	AGC	2690	*1	14.77	96.72	0.09230	0.510356	6	−44.51	−8.41
EKC02-34	Ngwempisi granite	Co. grained granite	26.5985	31.1524	AGC	2730	**3	22.32	136.33	0.09899	0.510445	6	−42.77	−8.24
EKC02-65	Hlatikulu granite	Med. grained granite	26.7349	31.4008	NGT	2729	2	16.62	94.46	0.10640	0.510609	6	−39.58	−7.90
EKC02-68	Sinceni pluton	Co. grained granite	26.6667	31.5505	NGT	2730	**3	10.10	48.56	0.12577	0.511032	6	−31.32	−6.26
BS04-13	Hlatikulu granite	Fi. grained granite	26.8651	31.2911	NGT	2730	*2	28.39	161.93	0.10599	0.510575	4	−40.24	−8.18
BS04-20	Hlatikulu granite	Med. grained granite	26.8543	31.2933	NGT	2733	2	19.29	112.78	0.10341	0.510573	6	−40.29	−7.37
BS04-21	Hlatikulu granite	Med. grained granite	26.8726	31.2727	NGT	2730	2	22.08	149.10	0.08954	0.510309	6	−45.42	−7.61
c. 3.1 Ga rocks														
KPV99-78	Nelspruit batholith	Med. grained granite	25.0772	30.1304	NBGB	3106	*4, 5	15.92	91.07	0.10568	0.510758	12	−36.67	−0.23
KPV99-79	Nelspruit batholith	Porphyritic granite	25.3599	30.9937	NBGB	3106	*4, 5	2.77	10.85	0.15456	0.512098	8	−10.53	6.39
KPV99-80	Nelspruit batholith	Med. grained granite	25.3599	30.9937	NBGB	3106	*4, 5	6.67	42.10	0.09584	0.510581	8	−40.13	0.24
KPV99-83	Nelspruit batholith	Med. grained granite	25.4739	30.9640	NBGB	3106	*4, 5	14.39	86.60	0.10049	0.510523	6	−41.25	−2.76
KPV99-84	Nelspruit batholith	Peg. dike	25.4739	30.9640	NBGB	3106	*4, 5	13.46	87.60	0.09292	0.510478	8	−42.14	−0.59
KPV99-86	Stentor pluton	Homo. granodiorite	25.6174	31.3064	NBGB	3106	*4, 5	6.34	40.61	0.09441	0.510489	8	−41.91	−0.96
KPV99-87	Stentor pluton	Fol. granodiorite	25.6174	31.3064	NBGB	3106	*4, 5	4.93	22.02	0.13539	0.511520	22	−21.80	2.80
KPV99-88	Stentor pluton	Pegamtitic granite	25.6174	31.3064	NBGB	3107	*4, 5	2.48	6.96	0.21529	0.513043	6	7.90	0.46
KPV99-89	Stentor pluton	Fol. granodiorite	25.6497	31.2426	NBGB	3107	5	6.69	42.85	0.09437	0.510527	6	−41.18	−0.21
KPV99-91	Stentor pluton	Late peg. dike	25.6497	31.2426	NBGB	3104	5	2.76	11.59	0.14406	0.511504	28	−22.12	−1.10
KPV99-91*	Stentor pluton	Late peg. dike	25.6497	31.2426	NBGB	3104	5	2.13	8.89	0.14516	0.511504	16	−22.12	−1.49
KPV99-102	Mpuluzi batholith	Med. grained granite	26.0834	30.7348	SST	3107	*4	1.25	8.52	0.08895	0.510190	8	−47.75	−4.64
WKC0045	Mpuluzi batholith	Med. grained granite	26.1565	30.7532	SST	3107	*4	15.15	81.39	0.11254	0.510754	6	−36.76	−3.08
WKC0055	Pigg's Peak batholith	Med. grained granite	26.0674	31.1830	AGC	3140	*6	5.63	35.18	0.09667	0.510474	6	−42.22	−2.09
EKC02-49	Mpuluzi batholith	Fi. Grained granite	26.1898	30.9604	SST	3107	*4	5.91	33.97	0.10510	0.510625	6	−39.27	−2.61
EKC02-55	Mpuluzi batholith	Med. grained granite	26.4645	31.0050	SST	3107	*4	5.57	30.68	0.10970	0.510699	6	−37.83	−3.01
EKC03-1	Pigg's Peak batholith	Med. grained granite	26.0333	31.1667	AGC	3140	*6	5.35	29.42	0.11003	0.510780	6	−36.23	−1.54
3.2–3.3 Ga rocks														
KPV 99-81	Nelspruit batholith	Amphibolite xenolith	25.3599	30.9937	NBGB	3250	**	11.17	62.06	0.10880	0.511127	14	−29.47	7.72
KPV 99-82	Nelspruit basement	Banded gneiss	25.4739	30.9640	NBGB	3258	*5	11.28	70.57	0.09665	0.510514	8	−41.43	0.60
KPV99-85	Kaap Valley pluton	Fol. grained tonalite	25.7688	31.0613	NBGB	3227	*4, 7	2.96	15.35	0.11668	0.510976	8	−32.43	0.88
KPV 99-90	Stentor basment	Banded gneiss	25.6497	31.2426	NBGB	3258	5	4.33	23.84	0.10992	0.510821	8	−35.44	1.02
KPV 99-90*	Stentor basment	Banded gneiss	25.6497	31.2426	NBGB	3258	5	4.30	23.83	0.10906	0.510801	8	−35.83	1.00
KPV99-92	Kaap Valley pluton	Fol. tonalite	25.7570	30.8452	NBGB	3227	*4, 7	3.33	16.73	0.12020	0.511078	6	−30.42	1.43
KPV99-94	Nelshoogte Pluton	Fol. granoriorite	25.8912	30.6235	NBGB	3236	5	0.70	3.97	0.10584	0.510763	10	−36.57	1.35
KPV99-95	Stolzburg pluton – young	Aplitic dike	26.0218	30.7442	SST	3213	*4, 5	3.07	18.82	0.09859	0.510550	6	−40.73	−0.09

Table 1 (Continued).

Sample description								Analytical data						
Name (a)	Rock unit (b)	Lithology (c)	Latitude (d)	Longitude (d)	Terr. (d)	Age (e)	Ref. (e)	[Sm] (f)	[Nd] (f)	$\frac{^{147}Sm}{^{144}Nd}$ (g)	$\frac{^{143}Nd}{^{144}Nd}$ (g)	± (h)	$\varepsilon_{Nd}(0)$ (i)	$\varepsilon_{Nd}(t)$ (i)
KPV99-97	Stolzburg pluton – young	Fi. grained granodiorite	26.0218	30.7442	SST	3213	*4, 5	2.71	15.53	0.10558	0.510645	8	−38.87	−1.14
KPV99-98	Stolzburg pluton – young	Fi. grained granodiorite	26.0218	30.7442	SST	3213	*4, 5	2.16	11.73	0.11133	0.510767	6	−36.50	−1.14
KPV99-101	Dalmein pluton	Med. grain granodiorite	26.0733	30.9007	SST	3216	*4	6.47	34.80	0.11250	0.510800	6	−35.86	−0.95
KPV99-103	Mpuluzi batholith	Mafic tonalite xenolith	26.0834	30.7348	SST	3200	**	5.45	25.46	0.12937	0.511202	8	−28.01	−0.10
WKC0068	Ancient Gneiss Complex	Late pegmatitic dike	26.3455	31.1453	AGC	3200	**	2.13	11.13	0.11587	0.510874	6	−34.41	−1.08
WKC0079	Usutu suite	Med. grain granodiorite	26.5216	31.2529	AGC	3227	*2	0.73	4.96	0.08919	0.510242	6	−46.73	−1.98
WKC0088	Vlakplaats plug	Med. grain granodiorite	26.1403	30.9809	SST	3230	5	3.47	19.97	0.10515	0.510651	8	−38.77	−0.65
EKC02-1	Dalmein pluton	Med. grain granodiorite	26.0884	30.9373	SST	3216	*4	8.02	52.03	0.09319	0.510413	6	−43.41	−0.49
EKC02-51	Kaap Valley pluton	Fol. tonalite	25.7578	30.8455	NBGB	3227	7	2.49	13.60	0.11081	0.510825	8	−35.36	0.38
EKC03-18	Usutu suite	Med. grain granodiorite	26.2841	31.3904	AGC	3186	2	2.37	14.13	0.10151	0.510611	6	−39.54	−0.32
AGC01-4	Usutu suite	Fol. tonalite	25.8952	31.3069	AGC	3226	6	7.62	41.98	0.10978	0.510716	6	−37.50	−1.36
EKC02-23	Usutu suite	Megacryst. granodiorite	26.2657	31.4450	AGC	3230	2	5.06	31.24	0.09796	0.510734	4	−37.15	4.00
EKC02-24	Usutu suite	Med. grained tonalite	26.2657	31.4450	AGC	3227	2	8.97	44.72	0.12123	0.510971	6	−32.52	−1.13
EKC02-32	Usutu suite	Med. grained tonalite	26.2841	31.3904	AGC	3232	2	8.87	60.36	0.08882	0.510217	6	−47.22	−2.28
EKC02-35	Usutu suite	Med. grain leucotonalite	26.6010	31.1666	AGC	3236	2	3.30	20.12	0.09923	0.510454	6	−42.61	−2.04
EKC03-21	Usutu suite	Med. grained tonalite	26.5533	31.3096	AGC	3232	2	2.65	16.33	0.09806	0.510482	4	−42.06	−1.00
EKC03-23	Usutu suite	Fol. tonalite	26.0547	31.1472	AGC	3230	2	8.27	41.80	0.11959	0.511074	6	−30.50	1.62
EKC03-33	Usutu suite	Megacryst. granodiorite	26.0540	31.1529	AGC	3227	2	10.61	60.24	0.10648	0.510587	6	−40.00	−2.46
EKC02-64	Nhlangano gneiss	Porph. banded gneiss	26.6675	31.3977	AGC/NGT	3266	2	2.68	20.87	0.07762	0.509969	6	−52.06	−1.92
EKC02-66	Nhlangano gneiss	Tonalitic banded gneiss	26.8003	31.3371	NGT	3266	2	1.68	10.22	0.09970	0.510542	6	−40.88	−0.03
EKC03-35	Nhlangano gneiss	Tonalitic banded gneiss	26.8760	31.2805	NGT	3300	2	5.89	37.81	0.09418	0.510358	6	−44.47	−0.84
EKC03-36	Nhlangano gneiss	Megacryst grano. gneiss	26.8764	31.2819	NGT	3300	2	3.99	22.40	0.10762	0.510689	6	−38.01	−0.10
EKC03-37	Nhlangano gneiss	Amphibolite banded gneiss	26.8763	31.2834	NGT	3300	2	4.93	19.61	0.15188	0.511574	6	−20.76	−1.70
BS04-6	Usutu suite	Med. grain granodiorite	26.5766	31.3455	AGC/NGT	3219	2	0.84	6.49	0.07788	0.510098	8	−49.54	−0.23
BS04-8	Usutu suite	Med. grain leucotonalite	26.5766	31.3455	AGC/NGT	3232	2	2.42	17.71	0.08256	0.510077	6	−49.96	−2.42
BS04-18	Nhlangano gneiss	Aplitic banded gneiss	26.8540	31.2987	AGC/NGT	3300	*2	6.91	38.56	0.10835	0.510715	6	−37.51	0.09
>3.45 Ga rocks														
KPV 99-96	Stolzburg pluton	Ton./grano. banded gneiss	26.0218	30.7442	SST	3445	5	3.16	16.76	0.11402	0.510788	8	−36.08	0.67
WKC0048	Ancient Gneiss Complex	Tonalitic banded gneiss	25.9098	31.3030	AGC	3664	*5, 8	19.60	143.33	0.08268	0.510192	6	−47.71	6.29
WKC0049	Ancient Gneiss Complex	Tonalitic banded gneiss	25.9098	31.3030	AGC	3550	*5, 8	6.18	22.70	0.16460	0.511676	6	−18.77	−4.10
WKC0056	Ancient Gneiss Complex	Tonalitic banded gneiss	26.0642	31.1831	AGC	3550	*5, 8	5.31	24.60	0.13047	0.511074	6	−30.51	−1.81
WKC0067	Ancient Gneiss Complex	Tonalitic banded gneiss	26.3455	31.1453	AGC	3500	*5, 8	14.01	72.84	0.11631	0.510815	6	−35.56	0.75
WKC0082	Ancient Gneiss Complex	Amphibolite banded gneiss	26.6747	31.1266	AGC	3550	*5, 8	6.60	24.72	0.16152	0.511757	6	−17.18	−1.07
WKC0083	Ancient Gneiss Complex	Peg. banded gneiss	26.6747	31.1266	AGC	3550	*5, 8	3.15	12.31	0.15466	0.511585	6	−20.53	−1.28
WKC0084	Ancient Gneiss Complex	Tonalitic banded gneiss	26.6747	31.1266	AGC	3550	*5, 8	2.52	12.71	0.11969	0.510879	4	−34.31	0.98
WKC0087	Steynsdorp pluton	Fol. tonalite-granodiorite	26.1779	30.9871	SST	3517	*4, 5	3.06	14.34	0.12905	0.511316	8	−25.79	4.96
AGC01-1	Tsawela gneiss	Tonalitic banded gneiss	26.7558	30.9794	AGC	3450	*9	3.22	16.38	0.11879	0.510850	6	−34.88	−0.20
AGC01-2	Ancient Gneiss Complex	Tonalitic banded gneiss	26.7141	31.0448	AGC	3550	*5, 8	1.06	7.57	0.08457	0.510182	8	−47.91	3.49
AGC01-5	Ancient Gneiss Complex	Tonalitic banded gneiss	25.8961	31.3104	AGC	3662	5	7.59	37.98	0.12073	0.510790	6	−36.05	−0.11

Table 1 (Continued).

Sample description								Analytical data						
Name (a)	Rock unit (b)	Lithology (c)	Latitude (d)	Longitude (d)	Terr. (d)	Age (e)	Ref. (e)	[Sm] (f)	[Nd] (f)	$\frac{^{147}Sm}{^{144}Nd}$ (g)	$\frac{^{143}Nd}{^{144}Nd}$ (g)	± (h)	$\varepsilon_{Nd}(0)$ (i)	$\varepsilon_{Nd}(t)$ (i)
EKC02-20	Phophonyane granite	Fi. grained fol. granite	25.8961	31.3104	AGC	3545	5	2.82	15.22	0.11188	0.510533	6	−41.06	−2.27
EKC02-40	Steynsdorp pluton	Fol. tonalite-granodiorite	26.1779	30.9604	AGC	3517	5	2.56	13.99	0.11051	0.510709	6	−37.63	1.50
EKC03-3	Stolzburg pluton	Homo. granodiorite	25.9740	30.7630	SST	3445	5	0.78	4.08	0.11639	0.510813	10	−35.61	0.09
BS04-7	Tsawela gneiss	Tonalitic banded gneiss	26.5766	31.3455	AGC	3411	2	3.86	22.96	0.10168	0.510433	6	−43.02	−1.21

(a) Sample name, grouped by approximate age. *Duplicate analysis.

(b) Name of rock unit or locality for rocks whose associations are difficult.

(c) Lithology of rock based on hand-sample description.

(d) Latitude and longitdue derived by hand-held global positioning system. Terr., terrane name from Fig. 1.

(e) Approximate U–Pb crystallization age in Ma, with references.

No symbol = exact rock sample dated; *# = same unit dated, but different sample in this study; **# = inferred same unit dated, based on rock type or map correlation; **no number = poor age constraints.

(1) Layer *et al.* (1989); (2) Schoene and Bowring (in revision); (3) Wilson (1982); (4) Kamo and Davis (1994); (5) Schoene *et al.* (2008); (6) Schoene and Bowring (2007); (7) Schoene *et al.* (2006); (8) Kröner *et al.* (1989); (9) Kröner and Tegtmeyer (1994).

(f) Concentrations in p.p.m., as determined by isotope dilution.

(g) Isotopic ratios corrected for mass fractionation (see text) and 100 pg Sm and Nd blank. Precision on Sm/Nd ratios ≤0.1%.

(h) 2-sigma standard error of fractionation-corrected ratio.

(i) Epsilon Nd value at the present day (0) and the time of crystallization (t), calculated as follows: $[(^{143}Nd/^{144}Nd)_{sample}/(^{143}Nd/^{144}Nd)_{CHUR}) - 1] \times 10^4$ see text for CHUR values used.

Nelshoogte and Kaap valley plutons of *c*. 3236 and 3227 Ma respectively, dates ranging from *c*. 3240 to 3280 Ma for the Badplaas orthogneisses and a *c*. 3.3 Ga xenolith from within a *c*. 3.1 Ga granitic batholith (Kamo and Davis, 1994; Kisters *et al*., 2006; Schoene *et al*., 2008). Bordering the SW BGB, orthogneiss complexes (e.g. the *c*. 3.45 Ga Stolzburg and the *c*. 3.52 Ga Steynsdorp complexes) were also intruded by *c*. 3.23 Ga syntectonic tonalitic to granodioritic magmas (Stevens *et al*., 2002; Dziggel *et al*., 2005; Schoene *et al*., 2008), which may be coeval with high-*P*, low-*T* metamorphism in this terrane (Kisters *et al*., 2003; Diener *et al*., 2005; Moyen *et al*., 2006). Schoene and Bowring (in revision) propose a NE–SW trending doubly vergent subduction zone from *c*. 3.28 to 3.22 Ga to account for the synchronicity of magmatism and deformation north and south of the BGB and the generation of the Nhlangano gneiss. Finally, the Neoarchean saw the eruption and deposition of the Pongola Supergroup *c*. 2.985 Ga and the intrusion of the Usushwana complex and associated mafic to ultramafic dikes *c*. 2.850 Ga (Fig. 1; Hegner *et al*., 1984).

On the basis of geochronology of exposed (meta)igneous rocks, we divided the study area into four areas (Fig. 1): The NBGB (rocks NW of the SIFS, NW of the BGB), the SST (the Stolzburg and Steynsdorp terrane), the AGC (Ancient Gneiss Complex including and the Usutu intrusive suite) and the NGT (the Nhlangano gneiss terrane and associated rocks). From these four areas, we collected plutonic and orthogneiss samples that range in composition from granite to gabbro with U–Pb crystallization ages between *c*. 3.66 and 2.7 Ga (Fig. 1). Sample descriptions and Sm–Nd analyses are presented in Table 1. Analytical methods are described in the Supporting Information.

Sm–Nd results and discussion

Nd isotopic map of the eastern Kaapvaal craton

To evaluate the role of older crust in the generation of exposed rocks, we examine the range of $\varepsilon_{Nd}(t)$ (ε_{Nd} at the time of crystallization) across the crustal transect for rocks of similar age. Magmatism occurred across the entire study area *c*. 3.2–3.3 Ga; *c*. 3.1 Ga granitic magmatism also extends from the AGC across the SST into the NBGB. Abundant *c*. 2.7 Ga magmatism occurred in the AGC and NGT only (Fig. 1). Figure 2 shows the sample locations projected onto a line trending 325° (approximately perpendicular to the NE–SW regional structural grain; cross-section line shown in Fig. 1) plotted against $\varepsilon_{Nd}(t)$. Both *c*. 3.2–3.3 and *c*. 3.1 Ga rocks show higher $\varepsilon_{Nd}(t)$ values in the NBGB. In the NBGB, *c*. 3.1 Ga samples have $\varepsilon_{Nd}(t) > -2$ and samples to the south have $\varepsilon_{Nd}(t) < -2$. For 3.2–3.3 Ga rocks, there are no samples with $\varepsilon_{Nd}(t) < 0$ in the NBGB, whereas $\varepsilon_{Nd}(t)$ for samples in other areas ranges from 0 to −3 (with two exceptions). No 3.2–3.3 Ga samples in the SST have $\varepsilon_{Nd}(t) < -2$. There is similar scatter in $\varepsilon_{Nd}(t)$ in 3.2–3.3 Ga samples on both sides of the boundary between the AGC and NGT, indicating that a similar previously enriched reservoir contributed to those rocks. Similarly, for *c*. 2.7 Ga granites, there is no difference in $\varepsilon_{Nd}(t)$ across the surface expression of that boundary.

The marked offsets in $\varepsilon_{Nd}(t)$ between coeval magmas in the NBGB, SST and AGC probably represent isotopically distinct crust/lithosphere in each terrane. Alternatively, the data may reflect similar crustal age, but different mixtures of enriched and depleted reservoirs in the resulting magmas. To test this, we also plotted the Sm/Nd ratios of rocks in Fig. 2 in each terrane. If elevated $\varepsilon_{Nd}(t)$ in the NBGB results from greater contribution of mantle-derived melt rather than from the absence of more evolved, low ε_{Nd} material at depth, there may be a correlation between relatively high $\varepsilon_{Nd}(t)$ and elevated Sm/Nd. Although some of the *c*. 3.1 Ga granite samples from the

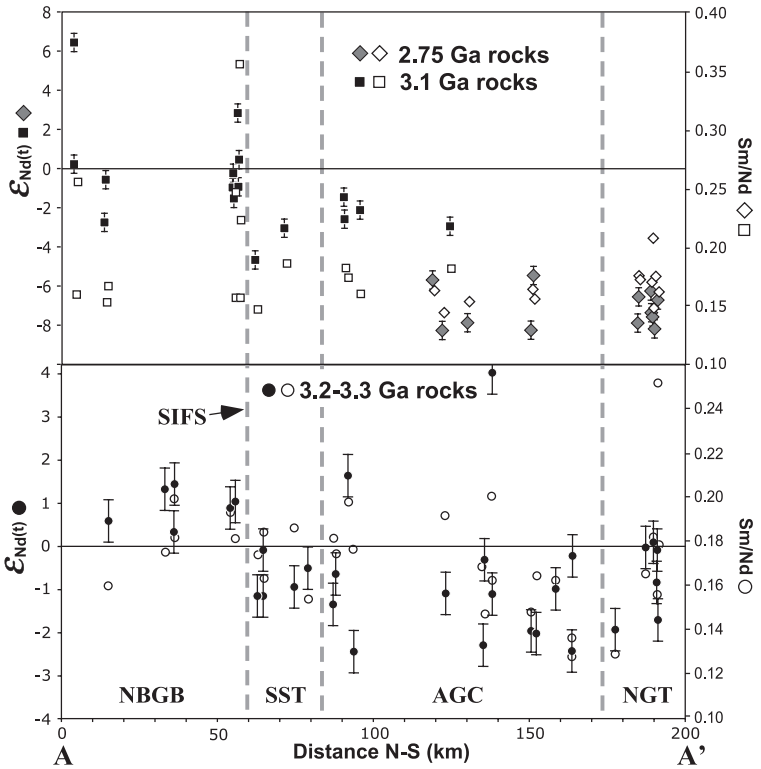

Fig. 2 Nd isotopic data and Sm/Nd plotted as a function of distance along the transect A–A′, shown in Fig. 1, for magmatic rocks 2.73, 3.1 and 3.2–3.3 Ga. Lithospheric boundaries inferred from surface geology indicated by dashed lines. See text for abbreviations and Fig. 1 for terrane locations in map view. Error bars on ε_{Nd} are fixed at ±0.5 at the 2-sigma level (see Supporting Information), and errors in Sm/Nd are smaller than symbol.

NBGB do show such a correlation, 3.2–3.3 Ga rocks show nearly identical Sm/Nd across the SIFS despite the offset in $\varepsilon_{Nd}(t)$ (Fig. 2). Thus, the 3.2–3.3 Ga granodiorites to tonalites probably inherited some component of older crust south of the SIFS.

Timescales of crustal growth and differentiation

$\varepsilon_{Nd}(t)$ values for rocks >3.45 Ga vary from −3 to +5 (ignoring two outliers), similar to that observed previously, which probably reflects the generation of these rocks by mixing mantle and older crustal components (Carlson *et al.*, 1983; Kröner and Tegtmeyer, 1994; Kröner *et al.*, 1996; Kröner, 2007). Similarities in $\varepsilon_{Nd}(t)$ between these and younger rocks south of the SIFS permit us to model this domain as a single lithospheric block, allowing evaluation of Sm–Nd evolution for nearly a billion years of cratonic evolution (*c.* 3.66–2.73 Ga). For rocks south of the SIFS, we have plotted $\varepsilon_{Nd}(t)$ and Sm/Nd as a function of time, using data from this study and from the literature (a total of 104 data points; Fig. 3). In general, $\varepsilon_{Nd}(t)$ of plutonic rocks define a linear array between 2.7 and 3.3 Ga, while $\varepsilon_{Nd}(t)$ values of rocks >3.45 Ga are more variable and plot mostly below an extension of that array to the depleted mantle curve (Fig. 3B). Metavolcanics of the Neoarchean Pongola Supergroup and the predominantly gabbroic Usushwana complex (Fig. 1) plot well above this array.

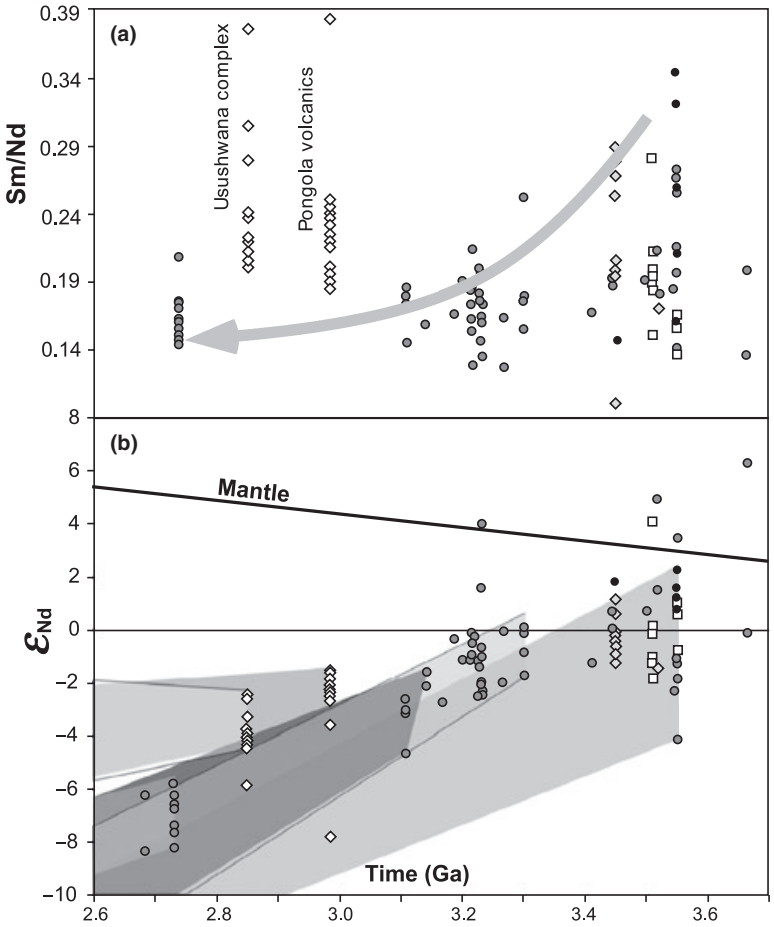

Fig. 3 Sm/Nd (A) and ε_{Nd} (B) values from this study and from the literature plotted as a function of crystallization age, for samples south of the SIFS. Gray circles, this study; black cirles, Carlson *et al.* (1983); white squares, (Kröner *et al.* (1996); gray diamonds, Kröner and Tegtmeyer (1994); white diamonds, Hegner *et al.* (1984). Shaded areas outline the evolution curves for rocks of the age that correspond to the oldest portion of a given trajectory. Depleted mantle curve results from drawing a line between 0 and +10 at 4500 and 0 Ma, respectively.

To quantify these trends, we calculated ε_{Nd} for each data point at five different dates corresponding to periods of magmatism between *c.* 2.73 and 3.25 Ga (Fig. 4). We then calculated the average ε_{Nd} at those times for (1) all the magmatic rocks of that age and (2) all the older host rocks present at that time, as a proxy for average crustal ε_{Nd}. For example, host rocks for *c.* 3.1 Ga magmas include both 3.2–3.3 Ga and >3.45 Ga rocks; Pongola and Usushwana rocks were not included as host rocks, because they are either volcanic or not regionally extensive respectively (Fig. 4). We find that at 3.25 Ga, $\varepsilon_{Nd}(t)$ of rocks south of the SIFS is elevated relative to the average crustal ε_{Nd} and therefore require input from a high ε_{Nd} source such as the mantle or older basaltic crust (Fig. 4). The Nd isotopic signatures of granitic magmas at *c.* 3.1 and 2.73 Ga can be entirely explained by *in situ* crustal melting with little or no mantle input. Pongola volcanics and the Usushwana intrusives also have elevated $\varepsilon_{Nd}(t)$ relative to the average crustal value, but still well below a depleted mantle value (which was ~+4; Fig. 3B; DePaolo, 1981; Bowring and Housh, 1995). Sm/Nd of Pongola and Usushwana rocks is also consistent with a contribution from a non-crustal source (Fig. 3A), in that they mostly plot above the *c.* 3.1 and 2.73 Ga granites. The other data follow a trend of lower Sm/Nd with time that is consistent with an increased importance of crustal melting and differentiation over time. The $\varepsilon_{Nd}(t)$ values of the Pongola and Usushwana rocks resulted from mixing mantle and crust, but those magmatic episodes had little effect on the bulk crustal Sm–Nd systematics in that the $\varepsilon_{Nd}(t)$ of 2.73 Ga granites can be explained entirely by melting average crust.

The above analysis assumes that calculated $\varepsilon_{Nd}(t)$ of >3.45 Ga basement rocks in the AGC are accurate, despite suggestions that some Archean rocks may have had their primary Sm/Nd altered through metamorphic processes based on expected $\varepsilon_{Nd}(t)$ when compared to Hf isotopic data (Gruau *et al.*, 1996; Vervoort *et al.*, 1996; Moorbath *et al.*, 1997). We

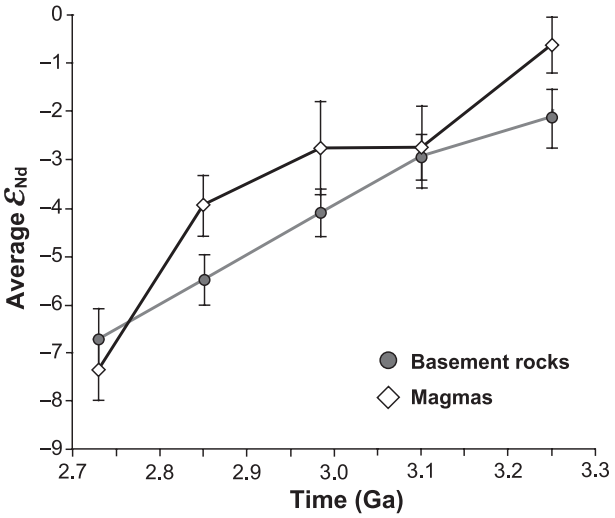

Fig. 4 crustal ε_{Nd} evolution for rocks south of the SIFS. Points and 2-sigma errors correspond to weighted mean values of ε_{Nd} for magmas of a given age and the basement rocks present at the time of crystallization. If the magma value is higher, it requires input from a depleted reservoir, if magma and basement rocks values are equal, then $\varepsilon_{Nd}(t)$ can be accounted for by intracrustal Nd recycling.

argue that this is not a problem in the above analysis because (1) the clustering of a vast majority of the rocks in the study between +2 and −3 over a large geographic area, (2) this cluster corresponds well to the range observed in low-grade metavolcanics at the base of the BGB (−2 to +2 at 3.45 Ga; Kröner and Tegtmeyer, 1994; Kröner *et al*., 1996; Chavagnac, 2004), and (3) the only regional metamorphic event documented is at *c*. 3.23 Ga (see references above), which corresponds to the starting point of the above analysis and thus the $\varepsilon_{Nd}(t)$ values at that time are unaffected. The few outliers that fall near or above the mantle curve in Fig. 3 may have had their Sm/Nd locally altered by metamorphic or fluid interaction processes, although it cannot be determined. We deem those samples worthy of future work, but regard the average of the cluster of analyses used above to be robust for the evolution of the crust as a whole.

Tectonic implications

Current models for the tectonic evolution of the BGB region are characterized by *c*. 3.23 Ga oblique subduction and accretion of an immature exotic terrane onto older lithosphere. These models are well-supported by metamorphic, petrological, geochronological, structural, and stratigraphic studies from the BGB and the flanking terranes (de Wit *et al*., 1992; Lowe, 1994; Clemens *et al*., 2006; Kisters *et al*., 2006; Moyen *et al*., 2006; Schoene *et al*., 2008; and references above). Our Sm–Nd isotopic mapping of the eastern Kaapvaal craton suggests that there were at least two distinct lithospheric blocks present *c*. 3.28–3.23 Ga, represented in Fig. 1 as the NBGB and the AGC + NGT ± SST. These new data, in combination with recently documented geochronology and field evidence south of the BGB, require that existing models be modified to include a doubly verging subduction zone to account for coeval magmatism and contractional deformation north and south of the BGB (Schoene and Bowring, in revision; Fig. 5). In such a model, from *c*. 3.28 to 3.24 Ga, the NBGB was formed and accreted onto pre-existing AGC and SST lithosphere, while the AGC hosted arc magmatism and deformation recorded in the Usutu intrusive suite and NGT. Consistently low $\varepsilon_{Nd}(t)$ across the AGC–NGT boundary requires older crust contributed to the NGT Nd-budget. Thus, the AGC is, or once was, more extensive than is presently exposed (Fig. 1). Inherited zircons ≤3.45 Ga in *c*. 3.24–3.28 Ga Nhlangano gneiss in the NGT support this hypothesis (Condie *et al*., 1996; Kleinhanns *et al*., 2003; Schoene and Bowring, in revision). The relationship between the SST and the AGC remains elusive, although slightly elevated $\varepsilon_{Nd}(t)$ of 3.2–3.3 Ga magmas

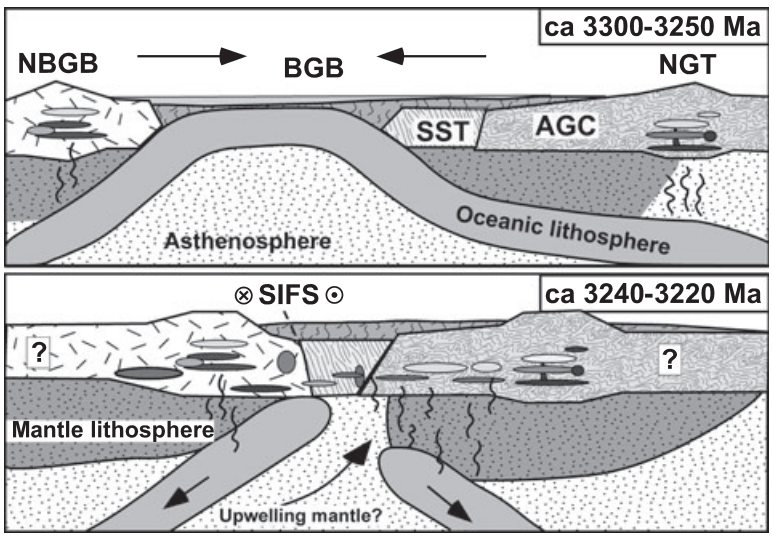

Fig. 5 Cartoon illustrating the *c*. 3.3–3.2 Ga tectonic evolution for basement rocks from the eastern Kaapvaal craton, after Schoene and Bowring (in revision), and references therein. Arrows in top panel show relative plate motions of the NBGB, and the AGC/SST. Continued subduction and hypothesized slab break-off led to melt generation by multiple mechanisms *c*. 3240–3220 Ma, resulting in a mixed crustal/mantle $\varepsilon_{Nd}(t)$ signature. See Fig. 1 for surface extent of lithospheric blocks and abbreviations.

compared to the AGC suggests the SST may represent one or more distinct crustal slivers, as has been hypothesized based on sedimentary and structural studies from within the BGB (Heubeck and Lowe, 1994; Lowe, 1994). Additionally, as pointed out by Schoene and Bowring (in press) and; Schoene *et al*. (2008), major structural modification of the crust *c*. 3.1 Ga needs to be addressed more closely in making *c*. 3.2 Ga paleoreconstructions of the eastern Kaapvaal craton.

Our analysis (Fig. 4) further supports a subduction origin for *c*. 3.28–3.22 Ga magmatism. $\varepsilon_{Nd}(t)$ for the *c*. 3.22–3.24 Ga Usutu intrusive suite in the AGC and the Nhlangano gneisses requires sources in the mantle and in older continental crust rather than melting lower continental crust exclusively (Figs 3 and 4). When combined with evidence for contractional deformation throughout the region and submarine basin closure in the BGB, a subduction model involving considerable crustal growth is the simplest explanation. Our data suggest that after *c*. 3.2 Ga, however, the eastern Kaapvaal craton behaved as a coherent lithospheric block dominated by crustal recycling through lower-crustal melting and little mantle Nd input. The proposed tectonic setting for the 3.1 Ga granites ranges from a transtensional to compressional to predominantly strike–slip kinematics (e.g. Kamo and Davis, 1994; de Ronde and de Wit, 1994; Westraat *et al*., 2005; Schoene *et al*., 2008). The geodynamic setting for *c*. 2.73 magmatism remains even more ambiguous, although we note the potential correlation in timing between the widespread Ventersdorp rifting event throughout the central craton (e.g. de Wit *et al*., 1992). In any case, these geochemical reorganizations of the crust were likely an important factor in the *c*. 3.1–2.7 Ga stabilization of the eastern Kaapvaal craton, in that it transported heat-producing elements (e.g. U, Th, K) into the upper crust, which can act to cool and strengthen the entire crustal column over time (see Schoene *et al*., 2008 and references therein).

Acknowledgements

The authors would like to thank B. Eglington, I. Schoenberg-Kleinhanns, A. Kröner, and an anonymous reviewer for insightful comments that improved the manuscript. Funding came in part from NSF EAR9526702 to S.B. This is AEON contribution #59.

References

Anhaeusser, C.R., 1983. Contributions to the geology of the Barberton Mountain Land. *Geol. Soc. S. Afr. Spec. Publ*., **9**, Johannesburg, 223p.

Bennett, V.C. and DePaolo, D.J., 1987. Proterozoic crustal history of the western United States as determined by neodymiom isotopic mapping. *GSA Bull*., **99**, 674–685.

Bowring, S.A. and Housh, T., 1995. The earth's early evolution. *Science*, **269**, 1535–1540.

Carlson, R.W., Hunter, D.R. and Barker, F., 1983. Sm-Nd age and isotopic systematics of the bimodal suite, ancient gneiss complex, Swaziland. *Nature*, **305**, 701–704.

Carlson, R.W., Boyd, F.R., Shirey, S.B., Janney, P.E., Grove, T.L., Bowring, S.A., Schmitz, M.D., Dann, J.C., Bell, D.R., Gurney, J.J., Richardson, S.H., Tredoux, M., Menzies, A.H., Pearson, D.G., Hart, R.A., Wilson, A.C. and Moser, D.E., 2000. Continental growth, preservation, and modification in Southern Africa. *GSA Today*, **10**, 1–8.

Chavagnac, V., 2004. A geochemical and Nd isotopic study Barberton komatiites (South Africa): implication for the Archean mantle. *Lithos*, **75**, 253–281.

Clemens, J.D., Yearron, L.M. and Stevens, G., 2006. Barberton (South Africa) TTG magmas: geochemical and experimental constraints on source-rock petrology, pressure of formation and tectonic setting. *Precambrian Res*., **151**, 53–78.

Compston, W. and Kröner, A., 1988. Multiple zircon growth within early Archean tonalitic gneiss from the Ancient Gneiss Complex, Swaziland. *Earth Planet. Sci. Lett*., **87**, 13–28.

Condie, K.C., Kröner, A. and Milisenda, C.C., 1996. Geochemistry and geochronology of the Mkhondo suite, Swaziland: evidence for passive-margin deposition and granulite facies metamorphism in the Late Archean of Southern Africa. *J. Afr. Earth Sci*., **21**, 483–506.

Davis, W.J. and Hegner, E., 1992. Neodymium isotopic evidence for the tectonic assembly of Late Archan crust in the Slave province, northwest Canada. *Contrib. Mineral. Petrol*., **111**, 493–502.

DePaolo, D.J., 1980. Crustal growth and mantle evolution: inferences from models of element transport and Nd and Sr isotopes. *Geochim. Cosmochim. Acta*, **44**, 1185–1196.

DePaolo, D.J., 1981. Neodymium isotopes in the Colorado Front Range and implications for crust formation and mantle evolution in the Proterozoic. *Nature*, **291**, 193–197.

DePaolo, D.J. and Wasserburg, G.J., 1976a. Inferences about magma sources and mantle structure from variations of $^{143}Nd/^{144}Nd$. *Geophys. Res. Lett*., **3**, 743–746.

Dickin, A.P., 2000. Crustal formation in the Grenville Province: Nd-isotope evidence. *Can. J. Earth Sci*., **37**, 165–181.

Diener, J.F.A., Stevens, G., Kisters, A.F.M. and Poujol, M., 2005. Metamorphism and exhumation of the basal parts of the Barberton greenstone belt, South Africa: constraining the rates of Mesoarchean tectonism. *Precambrian Res*., **143**, 87–112.

Dziggel, A., Armstrong, R.A., Stevens, G. and Nasdala, L., 2005. Growth of zircon and titanite during metamorphism in the granitoid-gneiss terrane south of the Barberton greenstone belt, South Africa. *Mineral. Mag*., **69**, 1019–1036.

Green, D.H., 1975. Genesis of Archean peridotitic magmas and constraints on Archean geothermal gradients and tectonics. *Geology*, **3**, 15–18.

Grove, T.L. and Parman, S.W., 2004. Thermal evolution of the Earth as recorded by komatiites. *Earth Planet. Sci. Lett. Front*., **219**, 173–187, doi: 10.1016/S0012-821X(04)00002-0.

Gruau, G., Rosing, M., Bridgewater, D. and Gill, R.C.O., 1996. Resetting of Sm-Nd systematics during metamorphism of > 3.7-Ga rocks: implications for isotopic models of early Earth differentiation. *Chem. Geol*., **133**, 225–240.

Hegner, E., Kröner, A. and Hofman, A.W., 1984. Age and isotope geochemistry of the Archean Pongola and Usushwana suites in Swasiland, southern Africa: a case for crustal contamination of mantle-derived magma. *Earth Planet. Sci. Lett*., **70**, 267–279.

Heubeck, C. and Lowe, D.R., 1994. Depositional and tectonic setting of the Archean Moodies Group, Barberton Greenstone Belt, South Africa. *Precambrian Res*., **68**, 257–290.

Jackson, M.P.A., 1984. Archean structural styles in the Ancient Gneiss Complex of Swaziland, southern Africa. In: *Precambrian Tectonics Illustrated* (A. Kröner and R. Greiling, eds), pp. 1–18. Schweizerbart'sche Verlagsbuchhandlung, Stuttgart.

Jackson, M.P.A., Eriksson, K.A. and Harris, C.W., 1987. Early Archean foredeep sedimentation related to crustal shortening: a reinterpretation of the Barberton Sequence, southern Africa. *Tectonophysics*, **136**, 197–221.

Kamo, S. and Davis, D.W., 1994. Reassessment of Archean crustal

development in the Barberton Mountain Land, South Africa, based on U-Pb dating. *Tectonics*, **13**, 167–192.
Kisters, A.F.M., Stevens, G., Dziggel, A. and Armstrong, R.A., 2003. Extensional detachment faulting and core-complex formation in the southern Barberton granite-greenstone terrain, South Africa: evidence for a 3.2 Ga orogenic collapse. *Precambrian Res.*, **127**, 335–378.
Kisters, A.F.M., Belcher, R.W., Poujol, M., Stevens, G. and Moyen, J.-F., 2006. A 3.2 Ga magmatic arc preserving 50 Ma of crustal convergence in the Barberton Terrain, South Africa. *Eos Trans. AGU*, **87**(52), Fall Meet. Suppl., Abstract V11D-0619.
Kleinhanns, I.C., Kramers, J.D. and Kamber, B.S., 2003. Importance of water for Archean granitoid petrology: a comparative study of TTG and potassic granitoids from Barberton Mountain Land, South Africa. *Contrib. Mineral. Petrol.*, **145**, 377–389.
Kröner, A., 2007. The Ancient Gneiss Complex of Swaziland and environs: record of early Archean crustal evolution in southern Africa. In: *Developments in Precambrian Geology*, Vol. 15 (M.J. van Kranendonk, H. Smithies and V. Bennett, eds), pp. 465–480. Earth's Oldest Rocks, Elsevier, Burlington.
Kröner, A. and Tegtmeyer, A., 1994. Gneiss-greenstone relationships in the Ancient Gneiss Complex of southwestern Swaziland, southern Africa, and implications for early crustal evolution. *Precambrian Res.*, **67**, 109–139.
Kröner, A., Compston, W. and William, I.S., 1989. Growth of early Archean crust in the Ancient Gneiss Complex of Swaziland as revealed by single zircon dating. *Tectonophysics*, **161**, 271–298.
Kröner, A., Byerly, G.R. and Lowe, D.R., 1991. Chronology of early Archean granite-greenstone evolution in the Barberton Moutain Land, South Africa, based on precise dating by single zircon evaporation. *Earth Planet. Sci. Lett.*, **103**, 41–54.
Kröner, A., Hegner, E., Wendt, J.I. and Byerly, G.R., 1996. The oldest part of the Barberton granitoid-greenstone terrain, South Africa: evidence for crust formation between 3.5 and 3.7 Ga. *Precambrian Res.*, **78**, 105–124.
Layer, P.W., Kröner, A., McWilliams, M. and York, D., 1989. Elements of the Archean thermal history and apparent polar wander of the eastern Kaapvaal Craton, Swaziland, from single grain dating and paleomagnetism. *Earth Planet. Sci. Lett.*, **93**, 23–24.
Lowe, D.R., 1994. Accretionary history of the Archean Barberton greenstone belt (3.55-3.22 Ga), Southern Africa. *Geology*, **22**, 1099–1102.
Lowe, D.R. and Byerly, G.R., 1999. *Geologic Evolution of the Barberton Greenstone Belt, South Africa*. Spec. Pap. 329. Geological Society of America.
Milisenda, C.C., Liew, T.C., Hofmann, A. and Kröner, A., 1988. Isotopic mapping of age provinces in precambrian high-grade terrains: Sri Lanka. *J. Geol.*, **96**, 608–615.
Moorbath, S., Whitehouse, M.J. and Kamber, B.S., 1997. Extreme Nd-isotope heterogeneity in the early Archaean – fact of fiction? Case histories from northern Canada and West Greenland. *Chem. Geol.*, **135**, 213–231.
Moyen, J.-F., Stevens, G. and Kisters, A.F.M., 2006. Record of mid-Archaean subduction from metamorphism in the Barberton terrain, South Africa. *Nature*, **44**, 559–662.
Nutman, A.P., Bennett, V.C., Kinny, P.D. and Price, R., 1993. Large-scale crustal structure of the northwestern Yilgarn craton, western Australia: evidence from Nd isotopic data and zircon geochronology. *Tectonics*, **12**, 971–981.
Richardson, S.H., Gurney, J.J., Erlank, A.J. and Harris, J.W., 1984. Origin of diamonds in old enriched mantle. *Nature*, **310**, 198–202.
de Ronde, C.E.J. and de Wit, M.J., 1994. Tectonic history of the Barberton Greenstone Belt, South Africa: 490 million years of Archean crustal evolution. *Tectonics*, **13**, 983–1005.
de Ronde, C.E.J. and Kamo, S., 2000. An Archean arc-arc collisional event: a short-lived (*ca.* 3 Myr) episode, Weltevreden area, Barberton greenstone belt, South Africa. *J. Afr. Earth Sci.*, **30**, 219–248.
de Ronde, C.E.J., de Wit, M.J. and Spooner, E.T.C., 1994. Early Archean (>3.2 Ga) Fe-oxide-rich, hydrothermal discharge veins in the barberton greenstone belt, South Africa. *GSA Bull.*, **106**, 86–104.
Schmitz, M.D., Bowring, S.A., de Wit, M.J. and Gartz, V., 2004. Subduction and terrane collision stabilized the western Kaapvaal craton tectosphere 2.9 billion years ago. *Earth Planet. Sci. Lett.*, **222**, 363–376.
Schoene, B. and Bowring, S.A., 2007. Determining accurate temperature-time paths in U-Pb thermochronology: an example from the SE Kaapvaal craton, southern Africa. *Geochim. Cosmochim. Acta*, **71**, 165–185.
Schoene, B. and Bowring, S.A., in press. *Rates and Mechanisms of Mesoarchean Magmatic Arc Construction, Eastern Kaapvaal Craton, Swaziland. GSA Bull.*
Schoene, B., Crowley, J.L., Condon, D.C., Schmitz, M.D. and Bowring, S.A., 2006. Reassessing the uranium decay constants for geochronology using ID-TIMS U-Pb data. *Geochim. Cosmochim. Acta*, **70**, 426–445.
Schoene, B., de Wit, M.J. and Bowring, S.A., 2008. Mesoarchean assembly and stabilization of the eastern Kaapvaal craton: A structural-thermochronological perspective. *Tectonics*, **27**, TC5010, doi: 10.1029/2008TC002267.
Stevens, G., Droop, G.T.R., Armstrong, R.A. and Anhaeusser, C.R., 2002. Amphibolite facies metamorphism in the Schapenburg schist belt: a record of the mid-crustal response to ~3.23 Ga terrane accretion in the Barberton greenstone belt. *S. Afr. J. Geol.*, **105**, 271–284.
Vervoort, J.D., Patchett, P.J., Gehrels, G.E. and Nutman, A.P., 1996. Constraints on early Earth differentiation from hafnium and neodymium isotopes. *Nature*, **379**, 624–627.
Viljoen, M.J. and Viljoen, R.P., 1969. An introduction to the geology of the Barberton, granite-greenstone terrain. *Geol. Soc. S. Afr. Spec. Publ.*, **9**, 1–20.
Westraat, J.D., Kisters, A.F.M., Poujol, M. and Stevens, G., 2005. Transcurrent shearing, granite sheeting and the incremental construction of the tabular 3.1 Ga Mpuluzi batholith, Barberton granite-greenstone terrane, South Africa. *J. Geol. Soc. Lond.*, **162**, 373–388.
Wilson, A.C., 1982. *1:250,000 Geological map of Swaziland*. Geological Survey Mines Department, Mbabane.
de Wit, M.J., 1982. Gliding and overthrust nappe tectonics in the Barberton greenstone belt. *J. Struct. Geol.*, **4**, 117–136.
de Wit, M.J. *et al.*, 1992. Formation of an Archean continent. *Nature*, **357**, 553–562.

Received 23 November 2008; revised version accepted 11 March 2009

Supporting Information

Additional Supporting Information may be found in the online version of this article:

Appendix S1 Analytical method.

Please note: Wiley-Blackwell are not responsible for the content or functionality of any supporting materials supplied by the authors. Any queries (other than missing material) should be directed to the corresponding author for the article.

